RSC Advances

PAPER

Cite this: *RSC Adv.*, 2016, **6**, 85634

Ordered intermetallic Pt–Cu nanoparticles for the catalytic CO oxidation reaction†

Govindachetty Saravanan,* Rohini Khobragade, Laxmi Chand Nagar and Nitin Labhsetwar

Received 3rd August 2016
Accepted 19th August 2016

DOI: 10.1039/c6ra19602k

www.rsc.org/advances

Platinum-based intermetallic nanoparticles (NPs), using the abundantly available element copper, with an average particle size of 4–5 nm on a γ-Al_2O_3 support were prepared successfully to reduce the consumption of Pt for the removal of CO through the catalytic oxidation reaction from flue gases. Intermetallic Pt–Cu NPs (Pt_3Cu, PtCu, and $PtCu_3$) with a Pt loading weight of 5 wt% were prepared on the γ-Al_2O_3 support by a simple wet impregnation method followed by calcination at various temperatures (500–800 °C) in a H_2 environment and they were characterized by powder X-ray diffraction analysis (pXRD), high resolution transmission electron microscopy (HR-TEM), selective area electron diffraction (SAED) method, *etc.* Despite the higher synthesis temperature of these intermetallic NPs, they were not agglomerated and formed a highly ordered intermetallic structure. The surface of the intermetallic Pt–Cu NPs with cubic-type structure (Pt_3Cu and $PtCu_3$) is enclosed of {200} facets, regardless of the significant difference in their compositions. Whereas the surface of rhombohedral-type intermetallic PtCu NPs is enclosed of {104} facets. Although the Pt-loading weight of these intermetallic NPs was the same, Pt_3Cu NPs showed a stable and enhanced catalytic activity compared to the other intermetallic PtCu and $PtCu_3$ NPs. Pt_3Cu NPs showed an onset and maximum conversion temperature of 50 and 125 °C, respectively. The intermetallic phase between Pt and Cu of Pt_3Cu NPs did not decompose; however, the intermetallic phase did decompose for PtCu and $PtCu_3$ NPs after catalytic CO oxidation. Unlike PtCu and $PtCu_3$ NPs, the Pt_3Cu NPs were not agglomerated and they were finely dispersed even after catalytic CO oxidation.

Introduction

Catalytic removal of carbon monoxide (CO) from flue gases is of primary importance for exhaust purification, fuel cell applications, *etc.*[1–4] Platinum group metals (PGM) still contribute to almost all catalytic-related applications owing to their superior performance in terms of activity, stability, relative strong against poisoning moieties, *etc.*[5] Nevertheless, there is an essential need to identify real-world catalysts as alternatives to PGM due to the huge gap between supply and demand.[6] The localized minerals of PGM in the world and their continuously increasing price due to the substantial usage of PGM for a variety of catalytic and other applications[7–9] are the main attributes for finding PGM alternatives. In addition, although PGM possess superior catalytic activities; however, they have certain limitations. In particular, they have poor activity at lower temperatures,[10] which would force researchers further to identify alternatives to PGM for low-temperature catalytic applications. It should be noted that most of toxic gases are emitted solely under low-temperature conditions, for instance automobile exhaust emissions (*i.e.*, cold start period).[10–12] Non PGM-based catalysts, including metal oxides, mixed metal oxides, and their shape-controlled forms, have been developed as alternatives to PGM;[13–19] however, they pose several limitations in terms of activity, long-term performance, stability, and poor sulfur-resistance. Therefore, considering the limitations of PGM and non-PGM-based catalysts, it would be reasonable to reduce the consumption of PGM. Therefore, considering the limitations of PGM and non-PGM-based catalysts, it would be reasonable to reduce the consumption of PGM by enhancing the catalytic activity with the same, or less, amount of PGM for targeted catalytic applications (*i.e.*, increasing the utilization efficiency) than the conventional PGM catalysts.

The performance of the catalysts can be enhanced by heating the catalysts externally and tuning the exhaust gas composition as well as catalytic properties of the catalysts. Tuning the exhaust gas composition and the external heating of the catalysts can significantly reduce the toxic emissions; however, this is accomplished at the expenditure of higher energy.[12] On the other hand, tuning the catalytic properties of the catalysts would allow us tailoring options, possibly with lower cost both

CSIR-National Environmental Engineering Research Institute (CSIR-NEERI), Nehru Marg, Nagpur 440 020, India. E-mail: g_saravanan@neeri.res.in

† Electronic supplementary information (ESI) available: pXRD profiles of γ-Al_2O_3 Pt/γ-Al_2O_3 and Pt- and Cu-precursors on γ-Al_2O_3 at various set temperatures, ICP-MS results. See DOI: 10.1039/c6ra19602k

in terms of composition as well as morphology. Therefore, tuning the catalytic properties of the catalysts may be one of the potential options to enhance the catalytic activity with a lower cost than that of conventional catalytic materials and/or other options to mitigate toxic emissions at a lower temperature.

Achieving of an intermetallic alloy phase between PGM and other transition metals (T) seems to be a promising strategy to reduce the consumption of PGM with superior performance owing to the changes in the atomic distance, electronic structure of component metals, d-band centers, bi-functional mechanism, *etc.*, which would consequently influence the adsorption behavior of the gases.[9,20–22] For example, CO interacts on a conventional Pt surface through a top, a bridge, and a tri-fold hollow interaction with higher adsorption energy. Eventually, a higher amount of energy is required to dissociate CO molecules from the Pt surface. However, CO interacts solely on the intermetallic phase of Pt–T through a non-competitive interaction (a top interaction) due to the different chemical nature of the adjacent atom to the Pt in the lattice of Pt–T. It has been proved that the intermetallic phase of Pt–Ti has approximately 20% less adsorption energy than that of pure Pt due to the changes in the electronic structure of Pt.[23–25] In addition, the component metals of the intermetallic phase, however, in some cases, provide adsorption sites for O_2, whereas Pt provides adsorption sites for CO (dual site mechanism) in the intermetallic alloys.[26,27] Intermetallic alloys possess both unique surface structures and bulk properties compared to that of usual alloys or component metals that are used extensively for superconductivity, hydrogen storage, and shape-memory related applications.[28–35] It has been proved that most of the intermetallic alloy phases with d-block elements showed improved catalytic activity and ameliorated stability under harsh catalytic conditions.[22,36]

Recently, the intermetallic alloy phase of Pt and Cu has become the focus of interest for several catalytic applications due to the improved catalytic performance over Pt alone, abundant availability of Cu, and their lower cost.[37–40] Intermetallic phases of Pt and Cu have been developed and used extensively as both cathode and anode catalysts for polymer electrolyte membrane fuel cell applications.[40–42] The core–shell Pt–PtCu nanotubes were prepared using Cu nanowires through a galvanic reaction followed by etching and annealing for the oxidation reaction of formic acid and oxygen reduction in fuel cell applications.[43,44] Concave Pt_xCu_y NPs were synthesized using molten salts of KNO_3 and $LiNO_3$ and showed significant catalytic activity for the electro-oxidation of methanol and formic acid as fuels.[45] Pt–Cu alloy concave nanocubes containing high-index facets were prepared by co-reduction of organometallic Pt- and Cu-precursors in the presence of capping agents and surfactants and exhibited enhanced methanol oxidation compared to commercial Pt/C for fuel cell applications. Nanoporous Cu–Pt core shell structures were achieved by the de-alloying of Cu/Al alloy followed by a galvanic replacement reaction for the methanol electro-oxidation reaction.[46] A 20 g batch of core–shell catalysts containing intermetallic $PtCu_3$ and Pt that were embedded in a carbon-support were realized as cathode materials through a galvanic reaction for a low-temperature fuel cell reaction.[47] Pt–Cu bimetallic NPs were prepared by the galvanic replacement reaction facilitated by high-intensity ultrasound at low temperatures without using any surfactants and they showed an enhancement in the oxygen reduction reaction by two-fold.[48] Intermetallic $PtCu_3$ NPs were prepared with different degrees of structural ordering on a graphitic carbon support for the reduction reaction of oxygen by the sol–gel method followed by annealing at various temperatures. The partially ordered structure showed higher catalytic activity compared to the disordered structure due to the retention time of Cu in the ordered structure and an intrinsic structural effect of the alloy.[49] Pt–Cu supported mesoporous graphitic carbon, as an oxygen reduction electrocatalyst, was prepared by a modified polyol process using shape-directing agents.[50] De-alloyed Pt–Cu core shell NPs as cathode catalysts were prepared by voltammetric de-alloying and showed a four-fold higher oxygen reduction performance than that of state-of-the-art Pt electrocatalysts.[51] The oxygen reduction reaction activity was tuned by controlled de-alloying of ordered intermetallic Cu_3Pt supported on carbon, which was prepared through the impregnation method followed by heat-treatment. The authors found that electrochemical de-alloying results a thin Pt-skin on an ordered Cu_3Pt core structure, but chemical leaching shows a spongy-like structure.[52,53] Pt–Cu bimetallic NPs < 3 nm in size were deposited on melem-modified carbon, followed by removing 90% of the copper, showed an enhanced electro-catalytic oxygen reduction reaction.[54] Bimetallic $PtCu_3$ NPs, as oxygen reduction catalysts, were prepared using a sonochemical synthesis method. Ultrasonic waves were subjected during reduction of precursors in a non-aqueous solution to synthesize $PtCu_3$ NPs.[55] Cu–Pt alloy nanocubes, with a broad range of compositions, were prepared using stabilizing and capping agents for electro-catalytic CO_2 reduction.[56] The composite film of Cu–Pt NPs and poly(8-hydroxyquinoline) was prepared on a glassy carbon electrode for the hydrogen evolution reaction through a galvanic reaction.[57] Al_2O_3 supported Pt–Cu catalysts, prepared through an impregnation technique, were used for a selective ring opening reaction of ethylcyclopentane. It was found that the changing of Cu-content modifies the catalytic mechanism of the ring opening reaction.[58] Photocatalytic hydrogen production from water was achieved at a higher production rate using 1-D CuPt nanorods, as a co-catalyst, that were synthesized using hexadecylamine and hexadecanoic acid as surface ligands.[59] Catalytic removal of CO from flue gases in a H_2-rich environment was examined using intermetallic PtCu for fuel cell applications.[5,60–65] Although alloys of Pt–Cu have been developed, most of the Pt–Cu alloys showed an alloy nature (*i.e.*, without ordered intermetallic structure), a wide size distribution range as well as wide Pt and Cu ratio range, the existence of Cu impurities, *etc.*, which may not be desired for achieving the targeted long-term catalytic performance.[66–68] In addition, complex synthesis methods, including a galvanic replacement reaction and using capping and shape-controlling agents, were adopted to prepare Pt–Cu alloys.[69–72] It should be noted that Pt forms three different ordered intermetallic phases with Cu namely: Pt_3Cu, PtCu, and $PtCu_3$ (Fig. 1). Although individual intermetallic phases of Pt–

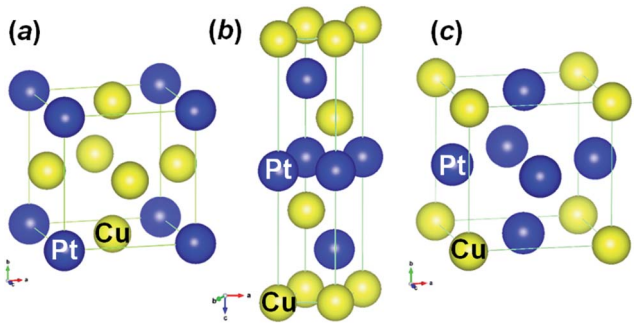

Fig. 1 Crystallographic structures of ordered intermetallic Pt_3Cu (a), PtCu (b) and $PtCu_3$ (c).

Cu have been studied, mostly for electro-catalytic applications, there has been no comparative study of these three ordered intermetallic Pt–Cu systems for thermal catalytic applications, which is of primary importance for both fundamental understanding as well as practical aspects of these promising intermetallic Pt–Cu phases. Therefore, the objective of this work is to develop a simple method to prepare the ordered intermetallic phases of Pt–Cu and access the possibility of catalytic centers for thermal catalytic applications using a model CO oxidation reaction.

Here in, we report the facile synthesis of an intermetallic phase of Pt–Cu (Pt_3Cu, PtCu, and $PtCu_3$) in the order of 4–5 nm through a simple wet-impregnation method followed by calcination at various temperatures under a H_2 environment. The formation of the intermetallic alloy phase of the synthesized Pt–Cu materials was examined by powder X-ray diffraction (pXRD) and selective area electron diffraction (SAED). The morphology of the intermetallic Pt–Cu NPs was examined using high-resolution transmission electron microscopy (HR-TEM). Inductively coupled plasma mass spectrometry (ICP-MS) was performed to quantify the amounts of Pt and Cu in the synthesized intermetallic Pt–Cu catalysts. The catalytic performance of these intermetallic phase Pt–Cu NPs was examined by the oxidation reaction of CO. The stability in terms of intermetallic phase and morphology of these intermetallic Pt–Cu NPs after catalytic reactions was examined systematically using pXRD and HR-TEM.

Experimental section

Materials and methods

The precursors, chloroplatinic acid hexahydrate ($H_2PtCl_6 \cdot 6H_2O$) (Pt assay: ≥37.50%) and copper(II) 2,4-pentanedionate ($C_{10}H_{14}CuO_4$) (98%) were purchased from Sigma Aldrich and Alfa Aesar, respectively, for the synthesis of the intermetallic alloy phase of Pt and Cu. γ-Al_2O_3 beads was purchased from Sasol, Germany. Al_2O_3 beads were crushed using a mixture and mortar and pestle each for 30 min to obtain a fine Al_2O_3 powder. High performance liquid chromatography grade methanol was purchased from Merck Ltd. H_2 gas (5% in N_2) as reducing agent, CO (5%), O_2 (99.99%), and He (99.998%) were purchased from Alchemie gases and chemicals Pvt. Ltd. The distilled water was prepared using a Millipore purifier system.

Synthesis of intermetallic Pt–Cu NPs on γ-Al_2O_3

The ordered intermetallic phase of Pt and Cu was synthesized using a wet-impregnation method followed by calcination at an elevated temperature in H_2 environment. 5 wt% Pt-loading was maintained for all intermetallic Pt–Cu catalysts. The stoichiometric ratio of Pt and Cu precursors for the desired intermetallic PtCu phase (3 : 1, 1 : 1, or 1 : 3) were dissolved in 50 ml of methanol and the composite solutions were stirred for 30 min at room temperature. 1 g of Al_2O_3 powder was added to the solution and stirred for 6 h. Methanol was evaporated by heating of the solution at 70 °C. The Pt and Cu precursors coated Al_2O_3 powder was ground for 15 min and then calcined at 300, 500, and 800 °C for 8 h in a H_2 environment. For the 1 g synthesis of intermetallic Pt–Cu intermetallic NPs on 1 g of γ-Al_2O_3 as catalysts, 0.1327 g (0.2562 mmol) of Pt-precursor and 0.0223 g (0.08519 mmol), 0.0671 g (0.2563 mmol), and 0.2010 g (0.7678 mmol) of Cu-precursor were weighed to prepare Pt_3Cu, PtCu, and $PtCu_3$ NPs, respectively, on the γ-Al_2O_3-support.

Characterization

The products were characterized by pXRD to identify the formation of an intermetallic alloy phase between Pt and Cu. The products were scanned in the 2θ range between 20 and 90° using a X-ray diffractometer (Rigaku: Miniflex-II-DD34863) using a source of CuKα radiation (λ = 0.15418 nm) operated at 30 kV and 15 mA at a step increment of 0.02° per 5 s. The morphology, including size and shape, of the synthesized products were obtained using a HR-TEM instrument (JEM-2100 F) at an acceleration voltage of 200 kV. The products were mixed with ethanol and sonicated until the solution become turbid and then dropped smoothly on carbon-coated Cu-grids (#200 mesh) followed by air drying at 40 °C. The SAED studies were performed to examine the crystal structure of the products in a randomly selected area. 10 mg of intermetallic Pt–Cu samples were digested using 10 ml of aqua regia to quantify the amounts of Pt and Cu of the synthesized catalysts by ICP-MS (PerkinElmer, NexION 300×). The products after the catalytic oxidation reaction of CO were further characterized by pXRD, TEM, particle size distribution, *etc.* to examine the influence of the catalysis reaction over the products.

Catalytic oxidation of CO

Catalytic CO oxidation reaction of the products was performed in a state-of-the-art fixed bed reactor equipped with a temperature programmed furnace, a gas chromatograph, and a thermal conductivity detector. An aliquot of 50 mg of the products was sandwiched between quartz wool in a quartz tube reactor (inner diameter = 5 mm) and subjected a feed gas containing CO gas (2%) and O_2 (5%) in He at a constant flow rate of 50 ml min^{-1}. The products were pre-conditioned in the H_2 environment at 250 °C for 1 h in prior to the CO oxidation reaction. The composition of the feed and effluent gases from the reactor were examined from room temperature to 350 °C. The

conversion efficiency of CO to CO_2 was estimated as a function of temperature by taking the ratio of the concentration of CO and CO_2. Triplicate experiments were performed, including the pre-treatment conditions, and the average values were taken to evaluate the catalytic performance of the intermetallic Pt–Cu catalysts.

Results and discussion

Fig. 2 shows the pXRD profiles of the products synthesized after calcination of the stoichiometric Pt and Cu precursors coated γ-Al_2O_3 in the presence of H_2 gas (5% in N_2) at various temperatures for 8 h. The characteristic diffraction peaks of the intermetallic Pt_3Cu phase were obtained at 23.1°, 32.9°, 40.6°, 47.2°, 68.9°, and 83.1° for the reflection planes of (100), (110), (111), (200), (220), and (311), respectively, ($Pm\bar{3}m$; $a = 0.3852$) (ICDD #04-017-6718) when the stoichiometric Pt- and Cu-precursors coated γ-Al_2O_3 was calcined at 800 °C, consistent with the simulated XRD lines shown in Fig. 2a. The satellite XRD peaks, due to the formation of an intermetallic phase, were not seen clearly in the pXRD profile owing to the overlapping of satellite peaks with the characteristic diffraction peaks of the γ-Al_2O_3 support (ESI, Fig. S1†) and also their weak intensity in nature compared to the major diffraction peaks of Pt_3Cu. The obtained diffraction peaks are, however, shifted to higher diffraction angles compared to the pure phase of Pt ($Fm\bar{3}m$; $a = 0.3924$ nm) due to the presence of Cu in the lattice of Pt (ESI, Fig. S1†). The lattice constant of Pt_3Cu was calculated to be 0.3852 nm, which was smaller than that of pure phase Pt. The formation of an intermetallic Pt_3Cu phase was also confirmed by the SAED studies (see Fig. 4d for the details). The characteristic diffraction peaks of ordered intermetallic PtCu phase ($R\bar{3}m$; $a = b = 0.270$ nm; $c = 1.2918$ nm) (ICDD #04-015-2415) were obtained when the stoichiometric Pt and Cu precursors coated γ-Al_2O_3 was calcined at 500 °C for 8 h, as shown in Fig. 2b. The weak, but yet recognizable, characteristic satellite diffraction peaks at 20.5°, 39.2°, 52.6°, and 71.1° for the reflection plans of (003), (101), (015), and (018), respectively, were observed, due to the formation of an intermetallic PtCu phase, in addition to the main characteristic diffraction peaks at 41.0°, 48.0°, 69.6°, and 84.3° for the reflection plane of (012), (104), (110), and (116), respectively, consistent with the simulated XRD lines as shown in Fig. 2b. The lattice constants of PtCu were calculated to be 0.240 and 1.2997 nm for a and c, respectively. It is well known that a PtCu system with ordered structure forms solely the rhombohedral structure.[73] Whereas, the PtCu system without an ordered structure forms a cubic structure ($Fm\bar{3}m$, $a = 3.7960$ nm) (JCPDS #48-1549). The formation of rhombohedral or cubic type structures is strongly dependent on the synthesis conditions. The cubic structure of PtCu generally shows the characteristic diffraction peaks without characteristic satellite peaks; however, they are shifted to higher diffraction angles compared to pure Pt due to the absence of an ordered structure (*i.e.*, alloy). Whereas, an intermetallic PtCu system shows the characteristic main diffraction peaks shifted to higher diffraction angles compared to Pt along with the characteristic satellite peaks due to the ordered structure (*i.e.*, intermetallic). Fig. 2c shows the characteristic diffraction peaks corresponding to $PtCu_3$ that were obtained when the stoichiometric Pt and Cu precursors coated γ-Al_2O_3 was calcined at 500 °C in a H_2 environment. In addition to the main diffraction peaks observed at 42.4°, 49.3°, 72.3°, and 87.6° for the reflection planes of (111), (200), (220), and (311), respectively, the characteristic satellite peaks at 24.1°, 34.3°, 55.1°, 61.5°, and 77.5° for the reflection planes of (100), (110), (210), (211), and (300) were also clearly obtained due to intermetallic $PtCu_3$ phase formation ($Pm\bar{3}m$; $a = 0.3692$ nm) (ICDD #03-065-3247), again consistent with the simulated XRD lines (Fig. 2c). The lattice constant for the $PtCu_3$ system was calculated to be 0.3695 nm, which is significantly smaller than the pure phase of Pt and other intermetallic Pt_3Cu systems having a cubic structure. It is worthy to mention that the lattice constant of the ordered intermetallic Pt–Cu system with cubic structure decreased linearly with the increase of Cu-content in Pt due to the contraction of lattice Pt upon intermetallic phase formation between Pt and Cu. The pure intermetallic Pt–Cu phase of Pt_3Cu, PtCu, and $PtCu_3$ were not obtained when the stoichiometric precursors were calcined at lower or higher temperatures than the set calcination temperatures (ESI, Fig. S2–S4†). Therefore, the calcination temperature is crucial for achieving the desired intermetallic phase between Pt and Cu under a H_2 environment. The temperature of the intermetallic phase formation decreased with the increase of Cu content in

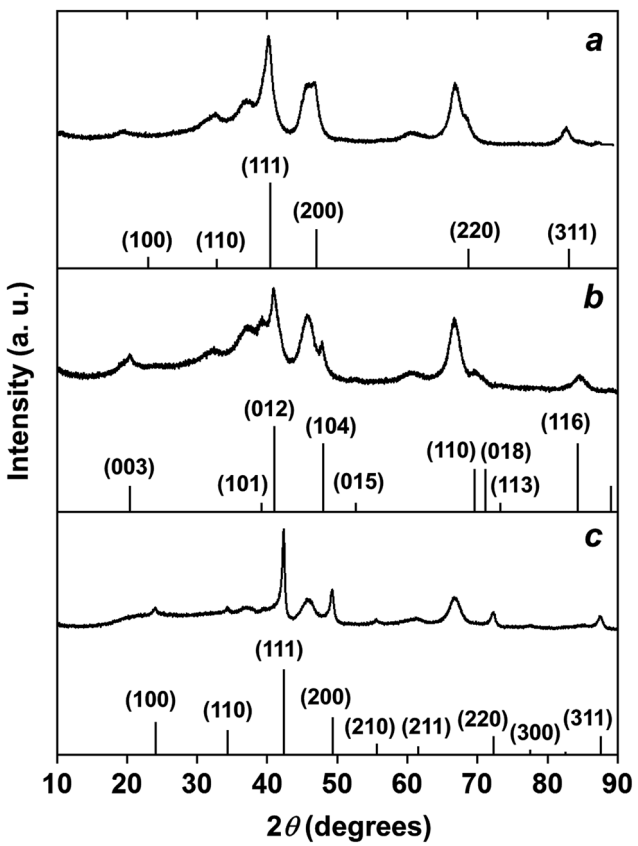

Fig. 2 X-ray diffraction profiles of Pt_3Cu/Al_2O_3 (a), $PtCu/Al_2O_3$ (b), and $PtCu_3/Al_2O_3$ (c). The simulated reference solid lines for these intermetallic Pt–Cu systems are shown at the bottom of each profile.

the Pt–Cu system. It should be noted that the synthesized products are free from the possible by-products, for instance, Pt, Cu, Cu-oxides, as no other diffraction peaks were obtained. These results infer that the selected synthesis methodology can aid the preparation of pure phase intermetallic Pt–Cu systems without forming any impurities.

TEM observation of the intermetallic Pt–Cu NPs on the γ-Al_2O_3 support was performed to examine their morphology, size, distribution, *etc.* The synthesized intermetallic Pt_3Cu NPs were semi-spherical in shape and they were well-dispersed on the γ-Al_2O_3 support, as shown in Fig. 3a. The size of the intermetallic Pt_3Cu NPs was in the range between 1 and 10 nm and the average particle size was centered at 4 nm (Fig. 3b). The intermetallic PtCu NPs also showed a similar trend to that of Pt_3Cu NPs where the PtCu NPs had a semi-spherical shape and they showed relatively poor dispersion on the γ-Al_2O_3 support (Fig. 3c). The particle size of PtCu NPs was in the range between 1 and 11 nm and the average particle size was 4 nm. The intermetallic $PtCu_3$ NPs also show the semi-spherical shape but they showed poor distribution on the γ-Al_2O_3 support compared to the other intermetallic Pt–Cu NPs. The particle size was in the range between 1 and 11 nm, almost as similar to the other intermetallic Pt–Cu NPs, and the average particle size was calculated to be 5 nm. It is worthy to note that the intermetallic Pt–Cu NPs on the γ-Al_2O_3 support were not agglomerated,

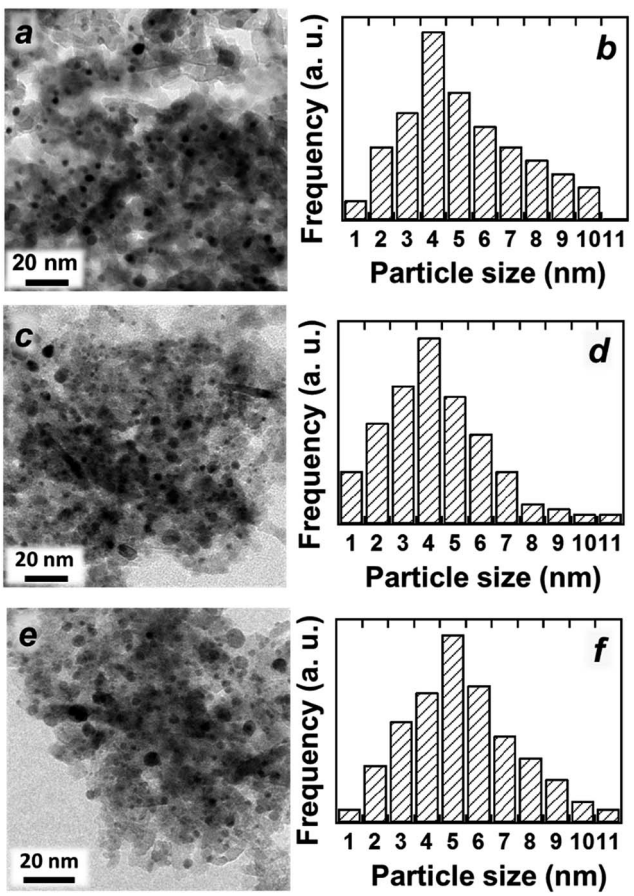

Fig. 3 TEM images and the particle size distributions of Pt_3Cu/Al_2O_3 (a, b), $PtCu/Al_2O_3$ (c, d), and $PtCu_3/Al_2O_3$ (e, f).

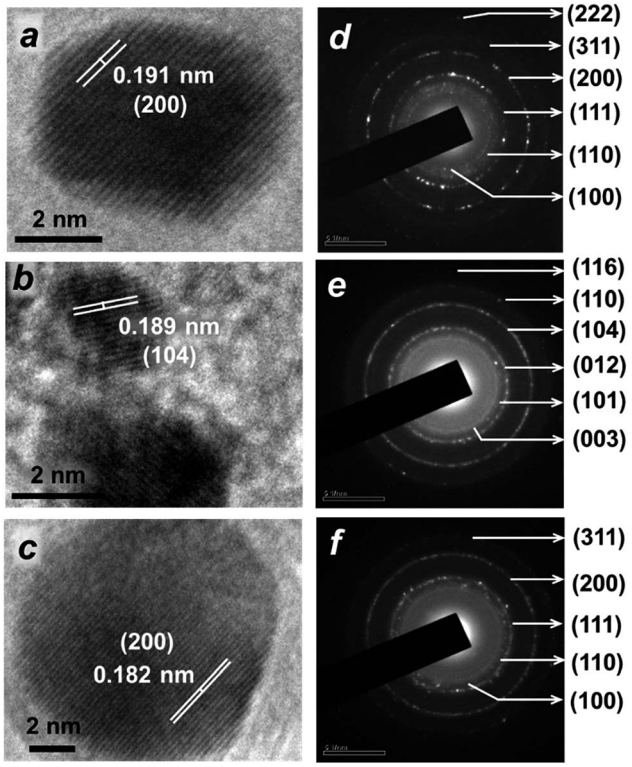

Fig. 4 HR-TEM images and SAED pattern of Pt_3Cu/Al_2O_3 (a, d), $PtCu/Al_2O_3$ (b, e), and $PtCu_3/Al_2O_3$ (c, f).

although they were synthesized at a higher temperature (500 and 800 °C) in the presence of H_2. Moreover, both the shape and the average particle size of Pt–Cu NPs on the γ-Al_2O_3 support did not change significantly, irrespective of the significant difference in composition of the intermetallic Pt–Cu NPs. These results infer that the finely dispersed intermetallic Pt–Cu NPs can be synthesized on the γ-Al_2O_3 support without any agglomeration at elevated temperatures in the presence of H_2.

HR-TEM observation of the intermetallic Pt–Cu NPs was performed to examine the atomic ordering, *d*-spacing, *etc.* Fig. 4a shows the HR-TEM image of a Pt_3Cu NP on the γ-Al_2O_3 support, which showed the atomic fringes with the *d*-spacing value of 0.191 nm corresponding to the {200} facet. PtCu NPs also showed the ordered structure with atomic fringes; however, they enclosed the {104} facet, as shown in the HR-TEM image (Fig. 4b). The *d*-spacing value of PtCu NPs from the atomic fringes was calculated to be 0.189 nm. Fig. 4c shows the HR-TEM image of a $PtCu_3$ NP on the γ-Al_2O_3 support. Clear atomic fringes were observed enclosing the {200} facet due to the ordered structures with a *d*-spacing value of 0.182 nm. $PtCu_3$ NP was embedded in the γ-Al_2O_3 support, as also clearly seen in Fig. 4c. It should be noted that the *d*-spacing of these intermetallic systems decreased with the increase of Cu-content in the Pt lattice, consistent with the reported results.[69] It seems that the selected synthesis conditions favor the formation of an intermetallic phase with the ordered structure, which was not altered even by the increase of Cu-content in the Pt lattice. Moreover, the ordered cubic-type structure of the Pt–Cu system

(Pt_3Cu and $PtCu_3$) favors the formation of the {200} facet on their surface under the selected synthesis conditions.

SAED studies were performed further on the intermetallic Pt–Cu NPs dispersed on the γ-Al_2O_3 support to ensure the formation of the intermetallic phase between Pt and Cu. Fig. 4d shows the SAED pattern of Pt_3Cu NPs that shows a set of strong concentric rings corresponding to the reflection planes of {111}, {200}, and {311}, that are consistent with the pXRD results. In addition to these strong concentric rings, a couple of weak concentric rings, corresponding to the reflection planes of {100} and {110}, were also observed. Although the characteristic satellite peaks for the Pt_3Cu intermetallic phase were not seen clearly in the pXRD profile (Fig. 2a), the characteristic reflection planes for the intermetallic Pt_3Cu phase were observed in the SAED pattern. Similarly, the weak concentric rings, corresponding to the reflection planes of {003} and {101}, were observed, due to the intermetallic phase of PtCu, in addition to the main reflection planes of {012}, {104}, {110}, and {116}, as can be seen clearly as strong concentric rings (Fig. 4e), consistent with the pXRD results (Fig. 2b). The SAED pattern of $PtCu_3$ NPs also clearly shows both the strong concentric rings for the reflection planes of {111}, {200}, and {311} and the weak concentric rings for the reflection planes of {100} and {110} (Fig. 4f), similar to Pt_3Cu NPs and consistent again with the pXRD results (Fig. 2c). Overall, the SAED patterns of the Pt–Cu NPs dispersed on the γ-Al_2O_3 support also ensure the formation of an intermetallic phase between Pt and Cu. These results infer that intermetallic Pt–Cu NPs with an average size of 4–5 nm can be synthesized on the γ-Al_2O_3 support without forming any impurities through the selected synthesis method. By considering the widely accepted factors, for instance alloying of Pt with the d-block elements, achieving a particle size smaller than 5 nm with an ordered structure would improve the catalytic performance of Pt. The present simple synthesis methodology enables one to prepare the potential intermetallic systems with an ordered structure at a smaller size on the targeted support for variety of catalytic applications. Oezaslan *et al.* also prepared the intermetallic Pt–Cu systems on a high surface area carbon support as electrode catalysts for the oxygen reduction reaction for fuel cell applications.[74]

ICP-MS experiments were performed to quantify the amounts of Pt and Cu in the synthesized intermetallic Pt–Cu catalysts (ESI, Table 1†). The estimated amounts of Pt for all the intermetallic Pt–Cu catalysts were in the range between 0.48 to 0.52 mg, closer to that of the calculated Pt amounts (0.5 mg), which was almost equal to 5 wt% with respect to the γ-Al_2O_3-support (1 g). Similarly, the amount of Cu was estimated to be 0.062, 0.156, and 0.53 mg, which is equal to 0.62, 1.56, and 5.3 wt% of Cu in the case of intermetallic Pt_3Cu, PtCu, and $PtCu_3$ catalysts, respectively. These results infer that the present synthesis method enables one to prepare the intermetallic Pt–Cu catalysts with the desired loading weight of Pt without any significant difference in the Pt amounts, even after synthesis.

CO oxidation, as a model reaction of these intermetallic Pt–Cu NPs on the γ-Al_2O_3 support, was performed carefully to examine their catalytic performance. All other conditions for the CO oxidation reaction, including pre-treatment, were maintained same throughout the catalytic evaluations. All these intermetallic catalysts showed catalytic activity in the tested temperature region; however, the onset and maximum CO conversion temperature were significantly different from each other. Pt_3Cu/Al_2O_3 showed the better catalytic CO oxidation performance compared to the other $PtCu/Al_2O_3$ and $PtCu_3/Al_2O_3$. Despite no significant difference in the particle size (4–5 nm) of these intermetallic Pt–Cu NPs on the γ-Al_2O_3 support, they showed a considerable difference in the catalytic CO oxidation performance (Fig. 5a). As can be seen in more detail in Fig. 5b, the onset temperature (CO conversion ≦5%) of Pt_3Cu/Al_2O_3 was 50 °C, which was significantly lower than that of $PtCu/Al_2O_3$ and $PtCu_3/Al_2O_3$, which showed the onset temperature at 125 and 175 °C, respectively. The maximum CO conversion temperature also shows a similar trend where Pt_3Cu/Al_2O_3 showed the maximum CO conversion temperature at 125 °C, which was again significantly lower than the other intermetallic Pt–Cu catalysts. $PtCu/Al_2O_3$ and $PtCu_3/Al_2O_3$ showed the maximum CO conversion temperatures at 225 and 275 °C, respectively. Although the Pt loading weight (5 wt%) of these intermetallic catalysts was the same, they showed a significant difference in the catalytic CO oxidation performance likely due to the difference in the electronic structure. Attempts will be made to study

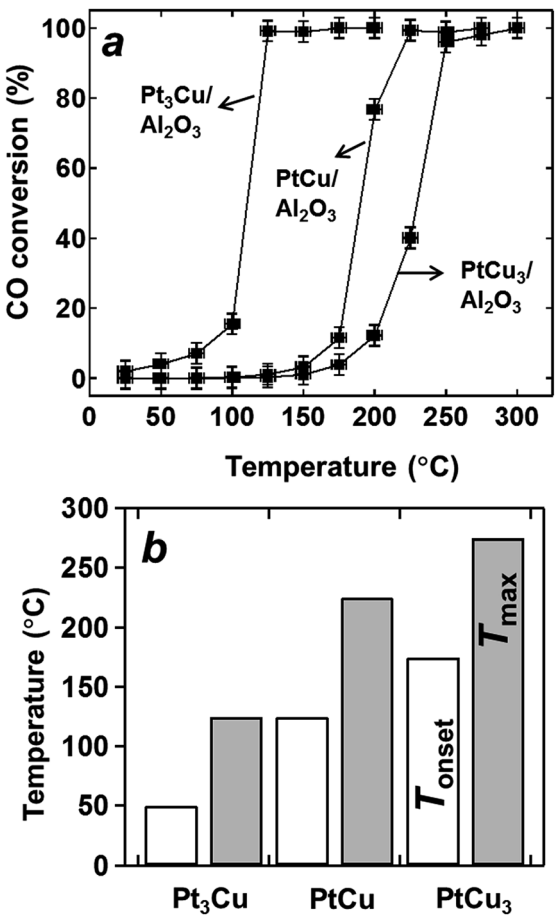

Fig. 5 Comparison of catalytic CO oxidation performance (a) and onset (open bar) and maximum conversion temperature (closed bar) (b) of Pt_3Cu/Al_2O_3, $PtCu/Al_2O_3$, and Pt_3Cu/Al_2O_3.

the electronic structure of these intermetallic Pt–Cu NPs to rationalize the observed difference in the catalytic performance.

pXRD analysis of the intermetallic Pt–Cu NPs on the γ-Al_2O_3 support after catalytic CO oxidation was performed to examine the stability of these catalysts. Fig. 6a shows the pXRD profile of Pt_3Cu/Al_2O_3 after catalytic CO oxidation, which shows the characteristic diffraction peaks of Pt_3Cu consistent with the pXRD profile of fresh Pt_3Cu/Al_2O_3 (Fig. 2a). $PtCu/Al_2O_3$ also shows no significant difference with the fresh $PtCu/Al_2O_3$, where the main characteristic diffraction peaks of PtCu were observed even after catalytic CO oxidation. It should be noted, however, that the characteristic satellite peaks due to the intermetallic phase of PtCu were not observed after CO oxidation (Fig. 6b), where they can be seen clearly in the pXRD profile of fresh $PtCu/Al_2O_3$ (Fig. 2b). Unlike Pt_3Cu/Al_2O_3 and $PtCu/Al_2O_3$, $PtCu_3/Al_2O_3$ showed significant changes both in terms of peak intensity as well as peak position in the pXRD profile after CO oxidation (Fig. 6c) compared to the fresh $PtCu_3/Al_2O_3$, where the characteristic main diffraction peaks were shifted to the lower diffraction angles, which are closer to pure phase Pt. The characteristic satellite peaks of $PtCu_3/Al_2O_3$ completely disappeared after the catalytic CO oxidation reaction due to the decomposition of the intermetallic phase of $PtCu_3$. In addition, the peak intensity of $PtCu_3$ decreased drastically after the catalytic CO oxidation reaction compared to fresh $PtCu_3/Al_2O_3$.

TEM analysis was further performed to examine the influence of catalytic conditions on the morphology, size of the particles and their dispersion, *etc.* of the intermetallic Pt–Cu on the γ-Al_2O_3 support after the CO oxidation reaction. Fig. 7 shows the TEM image of Pt_3Cu/Al_2O_3, $PtCu/Al_2O_3$, and $PtCu_3/Al_2O_3$ and their particle size distribution after the CO oxidation reaction. No significant changes in terms of morphology as well as particle size distribution were observed in the case of Pt_3Cu/Al_2O_3 after catalytic CO oxidation. The Pt_3Cu NPs are well dispersed and had a semi-spherical shape that was virtually same as fresh Pt_3Cu/Al_2O_3 (Fig. 3a), as shown in Fig. 7a. The size of the Pt_3Cu NPs on the γ-Al_2O_3 support was also not changed at all and ranged between 1 and 10 nm with an average Pt_3Cu NPs size centered at 4 nm. There was virtually no difference in terms of the morphology observed in the case of $PtCu/Al_2O_3$, where the PtCu NPs also showed a semi-spherical shape, similar to fresh $PtCu/Al_2O_3$ (Fig. 7c). However, the PtCu NPs were relatively agglomerated compared to the fresh PtCu NPs (Fig. 3c) after catalytic CO oxidation. The particle size was in the range between 1 and 15 nm and the average particle size was centered at 6 nm, as shown in Fig. 7d. Notably, the $PtCu_3$ NPs were largely agglomerated on the γ-Al_2O_3 support and the semi-spherical shaped particles of the fresh $PtCu_3$ (Fig. 3e) were changed in to various shapes after the catalytic CO oxidation (Fig. 7e). The size of the particles was widely distributed, which was in the range between 7 and 32 nm. These results unambiguously suggest that Pt_3Cu NPs are stable in terms of their intermetallic phase, size, morphology, dispersion, *etc.* on the γ-Al_2O_3 support compared to the other intermetallic PtCu and $PtCu_3$ NPs after catalytic CO oxidation.

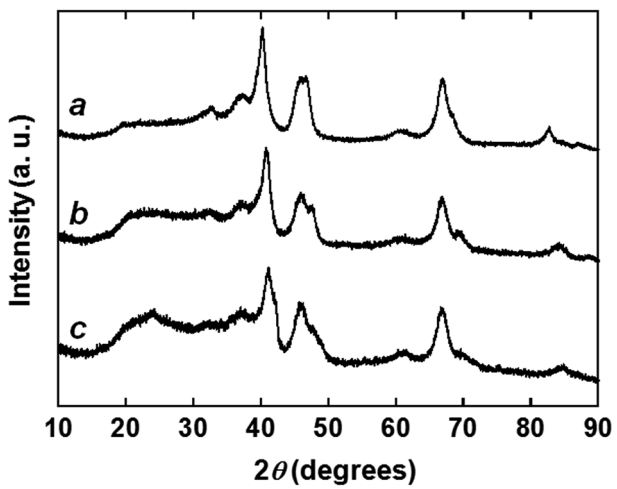

Fig. 6 X-ray diffraction profiles of Pt_3Cu/Al_2O_3 (a), $PtCu/Al_2O_3$ (b), and Pt_3Cu/Al_2O_3 (c) after catalytic CO oxidation.

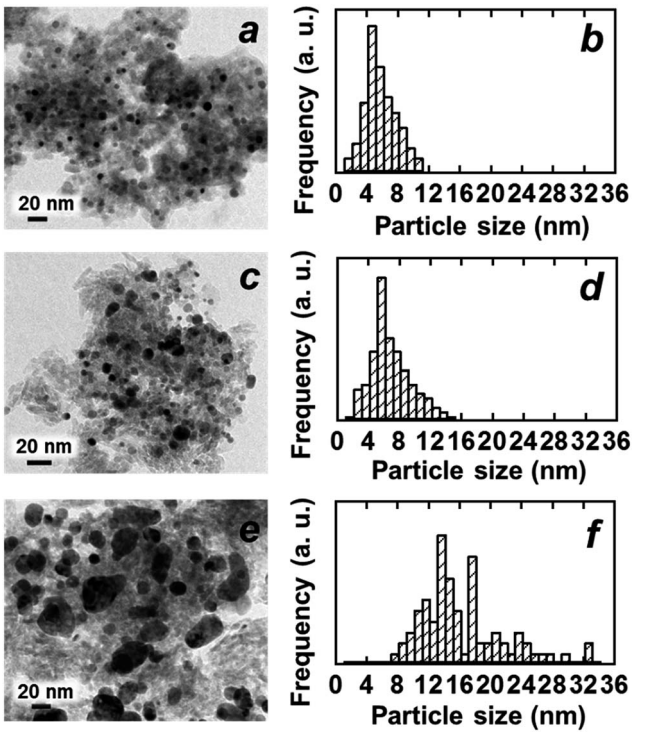

Fig. 7 TEM images and the particle size distribution of Pt_3Cu/Al_2O_3 (a, b), $PtCu/Al_2O_3$ (c, d), and Pt_3Cu/Al_2O_3 (e, f) after catalytic CO oxidation.

Conclusions

Intermetallic Pt–Cu (Pt_3Cu, PtCu, and $PtCu_3$) NPs were successfully prepared on the γ-Al_2O_3-support without any impurities through the wet-impregnation method *via* coating of the stoichiometric Pt and Cu precursors onto the γ-Al_2O_3 support followed by treating them at elevated temperature under a H_2 environment. The semi-spherical intermetallic Pt–Cu NPs, with an average size of 4–5 nm, are well dispersed on the γ-Al_2O_3 support regardless of the significant difference in

their composition. Despite the higher synthesis temperature, the cubic structure of Pt_3Cu and $PtCu_3$ NPs are not agglomerated and forms highly ordered intermetallic structures. The surface of these intermetallic NPs are enclosed by the {200} facet, whereas the rhombohedral structure of PtCu has the {104} facet on its surface. Pt_3Cu/Al_2O_3 catalysts showed the best catalytic performance for the oxidation reaction of CO in terms of onset as well as maximum conversion temperature among the other intermetallic $PtCu/Al_2O_3$ and $PtCu_3/Al_2O_3$ catalysts. Pt_3Cu NPs are stable in terms of the crystal structure, morphology, *etc.* compared to the other PtCu and $PtCu_3$ NPs after the catalytic CO oxidation reaction. The dispersion of Pt_3Cu NPs on the γ-Al_2O_3 support was virtually unchanged after the catalytic CO oxidation reaction; but, it did change for PtCu and $PtCu_3$ NPs. The reported synthesis method (*i.e.*, achieving of the ordered intermetallic Pt–Cu systems with smaller size) can be extended to the other order intermetallic systems that can find the other catalytic- and optical-related applications.

Acknowledgements

Dr G. Saravanan gratefully acknowledge Science and Engineering Research Board (SERB), Department of Science & Technology (DST), India for the financial support under young scientist scheme (SB/FT/CS-151/2013). KRC No. KRC\2016\MAY\EMD\6.

Notes and references

1 H. C. Yao and Y. F. Y. Yao, *J. Catal.*, 1984, **86**, 254–265.
2 C. Lamy, E. M. Belgsir and J.-M. Léger, *J. Appl. Electrochem.*, 2001, **31**, 799–809.
3 B. Du and Y.-Y. Tong, *J. Phys. Chem. B*, 2005, **109**, 17775–17780.
4 Y.-Y. Tong, H. S. Kim, P. K. Babu, P. Waszczuk, A. Wieckowski and E. Oldfield, *J. Am. Chem. Soc.*, 2002, **124**, 468–473.
5 S. H. Oh and R. M. Sinkevitch, *J. Catal.*, 1993, **142**, 254–262.
6 J. Matthey, *PGM Market Report*, May 2015, pp. 1–38.
7 A. Chen and P. Holt-Hindle, *Chem. Rev.*, 2010, **110**, 3767–3804.
8 H. A. Gasteiger and N. M. Markovic, *Science*, 2009, **324**, 48–49.
9 V. R. Stamenkovic, B. Fowler, B. S. Mun, G. Wang, P. N. Ross, C. A. Lucas and N. M. Markovic, *Science*, 2007, **315**, 493–497.
10 R. J. Farrauto and R. M. Heck, *Catal. Today*, 1999, **51**, 351–360.
11 R. S. D. Bosteels, *Platinum Met. Rev.*, 2002, **46**, 37.
12 M. Skoglundh and E. Fridell, *Top. Catal.*, 2004, **28**, 79–87.
13 P. Thormählen, E. Fridell, N. Cruise, M. Skoglundh and A. Palmqvist, *Appl. Catal., B*, 2001, **31**, 1–12.
14 Y.-F. Y. Yao, *J. Catal.*, 1975, **36**, 266–275.
15 G. Neri, G. Rizzo, S. Galvagno, A. Donato, M. G. musolino and R. Pietropaolo, *Appl. Catal., B*, 2001, **42**, 381–391.
16 Y. Teraoka, K. Kanada and S. Kagawa, *Appl. Catal., B*, 2001, **34**, 73–78.
17 Y. Wei, Z. Zhao, X. Yu, B. Jin, J. Liu, C. Xu, A. Duan, G. Jiang and S. Ma, *Catal. Sci. Technol.*, 2013, **3**, 2958–2970.
18 E. S. J. Lox, B. H. Engler, F. J. Janssen, R. L. Garten, R. A. Dalla Betta, J. C. Schlatter, Z. Ainbinder, L. E. Manzer, M. J. Nappa, V. N. Parmon and K. I. Zamaraev, in *Environmental Catalysis: Handbook of Heterogeneous Catalysis*, ed. G. Ertl, H. Knözinger and J. Weitkamp, Wiley-VCH, Weinheim, 1997, p. 1581.
19 A.-A. A. Said, M. M. M. Abd El-Wahab, S. A. Soliman and M. N. Goda, *Process Saf. Environ. Prot.*, 2016, **102**, 370–384.
20 V. R. Stamenkovic, B. S. Mun, M. Arenz, K. J. J. Mayrhofer, C. A. Lucas, G. Wang, P. N. Ross and N. M. Markovic, *Nat. Mater.*, 2007, **6**, 241–247.
21 J. Greeley, I. E. L. Stephens, A. S. Bondarenko, T. P. Johansson, H. A. Hansen, T. F. Jaramillo, J. Rossmeisl, I. Chorkendorff and J. K. Norskov, *Nat. Chem.*, 2009, **1**, 552–556.
22 H. Abe, H. Yoshikawa, N. Umezawa, Y. Xu, G. Saravanan, G. V Ramesh, T. Tanabe, R. Kodiyath, S. Ueda, N. Sekido, Y. Yamabe-Mitarai, M. Shimoda, T. Ohno, F. Matsumoto and T. Komatsu, *Phys. Chem. Chem. Phys.*, 2015, **17**, 4879–4887.
23 U. Bardi, D. Dahlgren and P. N. Ross, *J. Catal.*, 1986, **100**, 196–209.
24 G. Saravanan, H. Abe, Y. Xu, N. Sekido, H. Hirata, S. Matsumoto, H. Yoshikawa and Y. Yamabe-Mitarai, *Langmuir*, 2010, **26**, 11446–11451.
25 H. Abe, F. Matsumoto, L. R. Alden, S. C. Warren, H. D. Abruña and F. J. DiSalvo, *J. Am. Chem. Soc.*, 2008, **130**, 5452–5458.
26 E. Antolini, J. R. C. Salgado and E. R. Gonzalez, *Appl. Catal., B*, 2006, **63**, 137–149.
27 X. Zhao, M. Yin, L. Ma, L. Liang, C. Liu, J. Liao, T. Lu and W. Xing, *Energy Environ. Sci.*, 2011, **4**, 2736–2753.
28 D. Weller, A. Moser, L. Folks, M. E. Best, W. Lee, M. F. Toney, M. Schwickert, J. U. Thiele and M. F. Doerner, *IEEE Trans. Magn.*, 2000, **36**, 10–15.
29 S. Sun, C. B. Murray, D. Weller, L. Folks and A. Moser, *Science*, 2000, **287**, 1989–1992.
30 C.-M. Kuo, P. C. Kuo and H.-C. Wu, *J. Appl. Phys.*, 1999, **85**, 2264.
31 M. Watanabe, T. Nakayama, K. Watanabe, T. Hirayama and A. Tonomura, *Mater. Trans., JIM*, 1996, **37**, 489–493.
32 D. Weller and M. F. Doerner, *Annu. Rev. Mater. Sci.*, 2000, **30**, 611–644.
33 S. D. Bader, *Rev. Mod. Phys.*, 2006, **78**, 1–15.
34 T. Komatsu and A. Tamura, *J. Catal.*, 2008, **258**, 306–314.
35 W. E. Wallace, *Chem. Tech.*, 1982, **12**, 752–754.
36 D. Xiang and L. Yin, *J. Mater. Chem.*, 2012, **22**, 9584–9593.
37 M. Bele, P. Jovanovic, A. Pavlisic, B. Jozinovic, M. Zorko, A. Recnik, E. Chernyshova, S. Hocevar, N. Hodnik and M. Gaberscek, *Chem. Commun.*, 2014, **50**, 13124–13126.
38 H. Zhao, C. Yu, H. You, S. Yang, Y. Guo, B. Ding and X. Song, *J. Mater. Chem.*, 2012, **22**, 4780–4789.
39 N. Hodnik, C. Jeyabharathi, J. C. Meier, A. Kostka, K. L. Phani, A. Recnik, M. Bele, S. Hocevar, M. Gaberscek

and K. J. J. Mayrhofer, *Phys. Chem. Chem. Phys.*, 2014, **16**, 13610–13615.
40 L. Su, S. Shrestha, Z. Zhang, W. Mustain and Y. Lei, *J. Mater. Chem. A*, 2013, **1**, 12293–12301.
41 C.-M. Zhu, A. Gao, Y. Wang and Y. Liu, *Chem. Commun.*, 2014, **50**, 13889–13892.
42 H. Zhao, C. Yu, H. You, S. Yang, Y. Guo, B. Ding and X. Song, *J. Mater. Chem.*, 2012, **22**, 4780–4789.
43 C. Du, M. Chen, W. Wang, Q. Tan, K. Xiong and G. Yin, *J. Power Sources*, 2013, **204**, 630–635.
44 L. Su, S. Shrestha, Z. Zhang, W. Mustaina and Y. Lei, *J. Mater. Chem. A*, 2013, **1**, 12293–12301.
45 H. Zhao, C. Yu, H. You, S. Yang, Y. Guo, B. Dinga and X. Song, *J. Mater. Chem.*, 2012, **22**, 4780–4789.
46 C. Xu, Y. Liu, J. Wang, H. Geng and H. Qiu, *ACS Appl. Mater. Interfaces*, 2011, **3**, 4626–4632.
47 M. Bele, P. Jovanovic, A. Pavlisic, B. Jozinovic, M. Zorko, A. Recnik, E. Chernyshova, S. Hocevar, N. Hodnik and M. Gaberscek, *Chem. Commun.*, 2014, **50**, 13124–13126.
48 Z. Sun, J. Masa, W. Xia, D. Konig, A. Ludwig, Z. Li, M. Farle, W. Schuhmann and M. Muhler, *ACS Catal.*, 2012, **2**, 1647–1653.
49 N. Hodnik, C. Jeyabharathi, J. Meier, A. Kostka, K. Phani, A. Recnik, M. Bele, S. Hocevar, M. Gaberscek and K. Mayrhofer, *Phys. Chem. Chem. Phys.*, 2014, **16**, 13610–13615.
50 G. Gupta, D. Slanac, P. Kumar, J. Wiggins-Camacho, X. Wang, S. Swinnea, K. More, S. Dai, K. Stevenson and K. Johnston, *Chem. Mater.*, 2009, **21**, 4515–4526.
51 P. Mani, R. Srivastava and P. Strass, *J. Phys. Chem. C*, 2008, **112**, 2770–2778.
52 D. Wang, Y. Yu, H. Xin, R. Hovden, P. Ercius, J. Mundy, H. Chen, J. Richard, D. Muller, F. DiSalvo and H. Abrun, *Nano Lett.*, 2012, **12**, 5230–5238.
53 D. Wang, Y. Yu, J. Zhu, S. Liu, D. Muller and H. Abrun, *Nano Lett.*, 2015, **15**, 1343–1348.
54 C. Zhu, A. Gao, Y. Wang and Y. Liu, *Chem. Commun.*, 2014, **50**, 13889–13892.
55 C. Gumeci, D. Cearnaigh, D. Casadonte and C. Korzeniewski, *J. Mater. Chem. A*, 2013, **1**, 2322–2330.
56 X. Zhao, B. Luo, R. Long, C. Wang and Y. Xiong, *J. Mater. Chem. A*, 2015, **3**, 4134–4138.
57 J. Raoof, R. Ojani, S. Esfeden and S. Nadimi, *Int. J. Hydrogen Energy*, 2010, **35**, 3937–3944.
58 M. Boutahala, B. Djellouli, N. Zouaoui and F. Garin, *Catal. Today*, 2004, **89**, 379–385.
59 F. Yu, X. Xu, C. Baddeley, R. Bellabarba, P. Lignier, R. Tooze, F. Fina, J. Irvine and W. Zhou, *CrystEngComm*, 2014, **16**, 714.
60 A. K. Santra and D. W. Goodman, *Electrochim. Acta*, 2002, **47**, 3595–3609.
61 C. Song, *Catal. Today*, 2002, **77**, 17–49.
62 T. Komatsu, M. Takasaki, K. Ozawa, S. Furukawa and A. Muramatsu, *J. Phys. Chem. C*, 2013, **117**, 10483–10491.
63 S.-I. Ito, T. Fujimori, K. Nagashima, K. Yuzaki and K. Kunimori, *Catal. Today*, 2000, **57**, 247–254.
64 J. Levec, in Opportunities in Catalytic Reaction Engineering. Examples of Heterogeneous Catalysis in Water Remediation and Preferential CO Oxidation, in *Chemical Engineering: Trends and Developments*, ed. M. A. Galán and E. M. Del Valle, John Wiley & Sons, Ltd, Chichester, UK, 2005, pp. 103–123.
65 A. Manasilp and E. Gulari, *Appl. Catal., B*, 2002, **37**, 17–25.
66 I. Dutta, M. K. Carpenter, M. P. Balogh, J. M. Ziegelbauer, T. E. Moylan, M. H. Atwan and N. P. Irish, *J. Phys. Chem. C*, 2010, **114**, 16309–16320.
67 G. Gupta, D. A. Slanac, P. Kumar, J. D. Wiggins-Camacho, X. Wang, S. Swinnea, K. L. More, S. Dai, K. J. Stevenson and K. P. Johnston, *Chem. Mater.*, 2009, **21**, 4515–4526.
68 P. Strasser, S. Koh, T. Anniyev, J. Greeley, K. More, C. Yu, Z. Liu, S. Kaya, D. Nordlund, H. Ogasawara, M. F. Toney and A. Nilsson, *Nat. Chem.*, 2010, **2**, 454–460.
69 C. Gumeci, D. U. Cearnaigh, D. J. Casadonte and C. Korzeniewski, *J. Mater. Chem. A*, 2013, **1**, 2322–2330.
70 Y. Qi, T. Bian, S.-I. Choi, Y. Jiang, C. Jin, M. Fu, H. Zhang and D. Yang, *Chem. Commun.*, 2014, **50**, 560–562.
71 F. Yu, X. Xu, C. J. Baddeley, R. M. Bellabarba, P. Lignier, R. P. Tooze, F. Fina, J. S. T. Irvine and W. Zhou, *CrystEngComm*, 2014, **16**, 1714–1723.
72 H. M. Abdel Dayem, *Platinum Met. Rev.*, 2007, **51**, 138–144.
73 K. Mitsui, M. Takahashi and T. Takezawa, *Philos. Mag. Lett.*, 1998, **77**, 49–57.
74 M. Oezaslan, F. Hasche and P. Srasser, *J. Electrochem. Soc.*, 2012, **159**, B444–B454.

